Acta Cryst. (1996). A**52**, 189–197

Almost Free Rotation of NH_3 Molecules in Crystals: Observation from a Maximum-Entropy Reconstruction of the Proton Density in $[Co(NH_3)_6](PF_6)_2$

PETRA SCHIEBEL,[a] WOLFRAM PRANDL,[a]* ROBERT PAPOULAR[b] AND WERNER PAULUS[b]

[a]*Institut für Kristallographie, Universität Tübingen, Charlottenstrasse 33, D-72070 Tübingen, Germany, and* [b]*Laboratoire Léon Brillouin, C E de Saclay, F-91191 Gif-sur-Yvette, France*

(*Received 22 February 1995; accepted 22 September 1995*)

Abstract

Accurate density data yield the primary information required for a thermodynamic model of molecular disorder. A detailed analysis of the structure from neutron Bragg data shows that the protons of the ammonia groups perform nearly unhindered rotations at room temperature as well as at 30 K. The nuclear density distribution is derived from a combination of conventional crystallographic split-atom density interpolation and maximum-entropy density reconstruction. The crystallographic density interpolation allows unique phases to be determined, *i.e.* phases that are independent of details of the model, for the measured Fourier components. MaxEnt reconstruction eliminates series-termination effects and provides for higher quality in the spatial resolution compared with standard Fourier maps. The proton density obtained in $[Co(NH_3)_6](PF_6)_2$ at both temperatures is concentrated on a plane perpendicular to the fourfold crystal axis and is found to be nearly circular, with a weak tetragonal contribution superimposed. This is a strong indication of nearly free uniaxial rotation in this compound. The proton density is analysed in terms of an anharmonic orientational potential, which couples rotational and translational motion. The nearly unhindered rotation in this compound is a consequence of the quasi-eightfold symmetry built up by the next-neighbour F atoms surrounding the NH_3 groups in their plane of rotation.

1. Introduction

Compounds of the family $M(NX_3)_6Y_2$ with M = Ni, Co; X = H, D and Y = Br, I, NO_3, PF_6 are isomorphous. In their high-temperature phase, they generally form a face-centred cubic lattice (space group $Fm\bar{3}m$), where the basic unit is a cube of Y ions that surround one $M(NX_3)_6$ octahedron (Fig. 1). The incompatibility of the molecular symmetry $3m$ of NH_3 with the symmetry $4mm$ of the lattice site gives rise to the orientational disorder found in these compounds. On cooling these compounds, one observes various phase transitions and it was suggested that they are triggered by the freezing of NH_3 groups (Bates & Stevens, 1969). However, $[Ni(NH_3)_6](PF_6)_2$ and $[Co(NH_3)_6](PF_6)_2$ are unique among these compounds because they do not show any phase transition. In addition, large tunnel splittings, 500 and 542 μeV, respectively, have been reported for these compounds (Kearley, Blank & Cockcroft, 1987). These observations are an indication for weak hindrance potentials and thus for nearly free rotation.

Although the metal hexaammine salts, in particular the nickel compounds, have been investigated with several different techniques including quasielastic neutron scattering (QNS), Raman scattering, NMR and calorimetric measurements (Janik, Janik, Migdal-Mikuli, Mikuli & Otnes, 1991), there is still considerable lack of structural data. In the high-temperature phases, the orientations of the ammine groups are usually described in terms of disorder over a number of different sites, while for the low-temperature phases a detailed crystallographic description is still missing.

The direct observation of the density of rotating molecules is, in principle, a standard crystallographic routine. The scattering density is obtained by calculating Fourier maps from phased neutron data sets. This classical technique carries an inherent drawback, namely the broadening of all details and inherent 'noise' by series-termination effects. The maximum-entropy reconstruction of the densities is, by its construction from the principles of probability theory, the method offering the

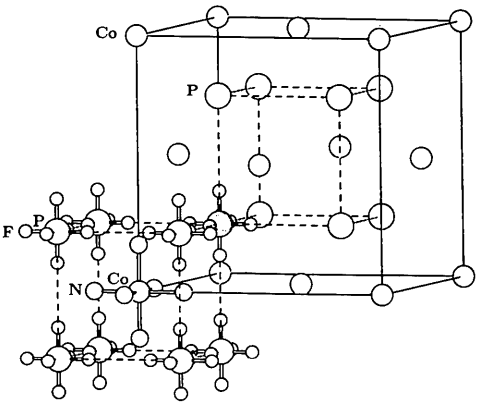

Fig. 1. Schematic view of the crystal structure. Each $[Co(NH_3)_6]$ cluster is centred in a cube built up of eight PF_6 octahedra.

ISSN 0108-7673

Table 1. *Eperimental details*

Chemical formula	$[Co(NH_3)_6](PF_6)_2$	
Chemical formula weight	451.00	
Crystal shape	Octahedral	
Crystal colour	Orange	
Sample volume (mm^3)	28	
Temperature	295 K	30 K
Crystal system	Cubic	Cubic
Space group	$Fm\bar{3}m$	$Fm\bar{3}m$
Lattice constant a (Å)	11.941 (2)	11.753 (2)
Cell volume ($Å^3$)	1702.7 (5)	1623.5 (5)
Z	4	4
D_x ($Mg\ m^{-3}$)	1.759	1.845
λ (neutrons) (Å)	0.8308	0.8308
No. of reflections for lattice parameters	20	20
θ range for lattice parameters (°)	10.0 – 30.0	10.0 – 30.0
θ_{max} (°)	37.34	37.45
Diffractometer	4-circle diffractometer 5C2 at LLB	
Scans	$\omega - 2\theta$	$\omega - 2\theta$
No. of measured reflections	945	1092
No. of observed reflections ($I > 2\sigma F$)	182	174
R_{int}	0.0597	0.0433
R_{sigma}	0.0430	0.0224

best estimate of densities. In particular, its application to the estimation of the density distribution arising from dynamically disordered molecules yields the high quality in spatial resolution that is necessary to interpret the density distribution originating from dynamically disordered molecules (Papoular, Prandl & Schiebel, 1992).

Indeed, applying MaxEnt to neutron data involves an extra technicality owing to the occurrence of negative scattering density coming from the H atoms, namely the use of a two-channel entropy. These two channels are introduced to reconstruct the positive and negative densities separately. We have used our own implementation of two-channel MaxEnt, which we have already applied in the past to reconstruct positive and negative magnetization densities from polarized neutron diffraction data. A detailed description of the latter is given (Papoular & Gillon, 1990*a*,*b*), where simulations are discussed along with examples from real data sets. Another implementation of two-channel MaxEnt has also been restored by Sakata *et al.* (1993) in the context of unpolarized neutron diffraction of a diatomic compound (TiO_2), involving scattering lengths of opposite signs.

In a recent study on a series of nickel hexaammine compounds in their cubic phases (Schiebel *et al.*, 1995), we obtained the scattering densities from the orientationally disordered protons and deuterons by Fourier techniques and observed a nuclear density distribution with four maxima on the corners of a square for the compounds with Y = Br, I, NO_3, whereas a nearly circular density distribution was found for $Y = PF_6$. All observed density distributions could consistently be explained as the consequence of rotation–translation coupling in an anharmonic crystal potential. The anharmonicity and the strength of the coupling depend on the type of anion present in the crystal frame and turned out to be very weak for the $[Ni(NH_3)_6](PF_6)_2$ compound.

With these results in mind, we started a neutron diffraction study on single crystals of $[Co(NH_3)_6](PF_6)_2$ and emphasized the accurate determination of the scattering density. Our ultimate goal is to interpret the disordered proton density by a thermodynamic model and to extract the crystal potential, which is the basis of the disorder.

This paper is organized as follows. Sample preparation and experimental set-up are given in §2. In §3, we report the results obtained by conventional crystallographic structure analysis. Our attempt was to determine the phases of the measured $|F_{hkl}| \simeq (I_{hkl})^{1/2}$. The data analysis concentrates on the evaluation of the proton density distribution by Fourier transformation and by maximum-entropy reconstruction (§4). In §5, the observed proton-density distribution is explained as the consequence of an anharmonic mean crystal potential and finally a model for the motion of the ammonia group is discussed.

2. Experimental

Single crystals were synthesized from aqueous solution. Samples were prepared by dissolving $[Co(NO_3)_2]\cdot 6H_2O$ in concentrated ammonia solution to give $[Co(NH_3)_6(OH)_2]$. Adding NH_4PF_6 and heating to 343 K yielded an oversaturated solution. By slowly cooling the solution down ($1\ K\ d^{-1}$) to room temperature, we observed the growth of single crystals with orange colour and octahedral shape.

Neutron diffraction measurements on single crystals at room temperature and at 30 K were performed on the four-circle diffractometer C2 at the hot source of the Orphee reactor in Saclay. Experimental details are given in Table 1. Absorption correction was found to be negligible. Extinction correction was included in the structure refinement (*SHELXL*93; Sheldrick, 1993) and also turned out to be negligibly small for both data sets.

3. Structure refinement

The main purpose of the classical refinement with Frenkel models is to determine a set of signs for the $|F_{hkl}|$ that is independent of details of the models. These signed F_{hkl}'s are then used to extract the pure proton density *via* a MaxEnt reconstruction.

The structure refinement is carried out with the program *SHELXL*93 (Sheldrick, 1993). We use the basic structural information (Fig. 1) of $[Co(NH_3)_6](PF_6)_2$: Co in 4(*a*), (0, 0, 0), P in 8(*c*), $(\frac{1}{4}, \frac{1}{4}, \frac{1}{4})$, F in 48(*g*), $(x, \frac{1}{4}, \frac{1}{4})$, N in 24(*e*), $(x, 0, 0)$, plus face centring.

The thermal motion of the F atoms at room temperature is found to be very large. The refinement of the room-temperature data was improved by allowing the F atoms to move from $(x, \frac{1}{4}, \frac{1}{4})$ to a general position by introducing split-atom positions for the F atoms. This

results in a reduction of the agreement factors by roughly 0.02.

The H atoms are treated by density interpolation. The basic idea behind density interpolation is to replace a disordered atom or molecule by a fictitious larger number of fractional atoms (split-atom model) or fractional groups (Frenkel or split-molecule model) undergoing harmonic motion (Fig. 2). A molecule placed in a general position results in 24 H-atom positions, *i.e.* 8 fractional molecules superimposed (model III). The threefold molecular symmetry combined with the fourfold site symmetry leads to at least 12 H-atom positions with occupational weight 0.25 if a molecular mirror plane coincides with one of the crystal mirror planes. Corresponding models are denoted by *0Y* and *XX*. However, the simplest model to account for hydrogen is a phenomenological split-atom model with just one H-atom site with occupational weight 0.375, which results in eight H-atom positions on a circle (model I).

In a first attempt, the ammonia molecule is treated as a rigid group, rotating around the respective Co—N bond, *i.e.* with its threefold axis aligned parallel to the fourfold axis. To locate the H atoms, *SHELXL93* allows one to calculate a difference scattering density around the circle that represents the loci of possible H-atom positions. The program takes, after local threefold averaging, the position of the maximum density as starting position for the H atoms. However, it turned out for both data sets that the scattering density on this circle shows four weak maxima and after threefold averaging is completely flat, *i.e.* constant. In successive refinement cycles, the H-atom positions do not converge but are shifted. The resulting agreement factors are independent of the actual H-atom positions on the circle. The 30 K data allow one to refine the NH_3 group with variable metric, yielding agreement factors $R(F^2 > 2\sigma F^2)_{30K} = 0.056$, $wR(F^2)_{30K} = 0.118$ for 13 refined parameters. The refined N—H bond length is $d_{N—H} = 1.024\,(6)$ Å. For the room-temperature data, the variable metric refinement turned out to be unstable. With fixed N—H bond length ($d_{N—H} = 1.03$ Å, 17 refined parameters), $R(F^2 > 2\sigma F^2)_{RT} = 0.103$, $wR(F^2)_{RT} = 0.196$ are obtained.

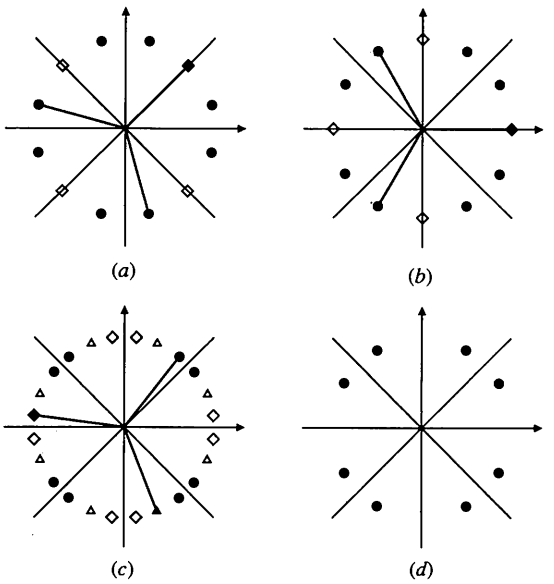

Fig. 2. Different Frenkel- and split-atom models used for the density interpolation of the disordered H atoms in the refinement with *SHELXL93*. (*a*) Model *XX*; (*b*) model *0Y*; (*c*) model III; (*d*) model I.

Next, the NH_3 group is allowed to tilt. This introduces two additional parameters. The resulting agreement factors are $R(F^2 > 2\sigma F^2)_{30K} = 0.049$, $wR(F^2)_{30K} = 0.107$ and $R(F^2 > 2\sigma F^2)_{RT} = 0.099$, $wR(F^2)_{RT} = 0.185$. The resulting N—H bond lengths are $d_{30K}^{N—H} = 1.031\,(4)$ Å and $d_{RT}^{N—H} = 1.033\,(7)$ Å. The deviation from the centre of the proton triangle to the fourfold axis r_c is found to be 0.062 (6) Å at 30 K and 0.065 (16) Å at 295 K. Thus, for both data sets, the tilt angle is found to be small, namely 1.4 (1)° (30 K) and 1.5 (1)° (RT).

Finally, we refined with anisotropically vibrating NH_3 groups (model III). Keeping the three H···H distances and the three N—H bonds equal and using 'rigid-bond' constraints for the anisotropic displacement parameters introduces nine constraints. For the room-temperature data, this model results in the best agreement factors. In the results derived from the data set at 30 K, two of the three H atoms occupy symmetry-equivalent positions and the third one is placed on the (0*yz*) position, which means that the refinement converged to model *0Y*. Therefore, the number of free parameters is reduced by introducing only one position with doubled occupancy for these two H atoms. Results are given in Tables 2 and 3. From these refinements, $d_{30K}^{N—H} = 1.021\,(14)$ and $d_{RT}^{N—H} = 1.057\,(9)$ Å are found. The centre of mass of the proton triangle at 30 K coincides with the fourfold axis $(x_c, y_c, z_c) = (0.2200\,(6), 0.0000\,(4), 0.0003\,(8))$, therefore, the tilt angle at 30 K is negligible [$\varphi_{30K} = 0.0\,(1)°$]. At room temperature, $(x_c, y_c, z_c) = (0.2160\,(26), -0.0012\,(14), -0.0047\,(15))$ and a small tilt angle [$\varphi_{RT} = 1.3\,(1)°$] is derived.

In addition to the rigid-body refinements, we refined the four different models (I, *0Y*, *XX*, III) without applying any bond-length constraints. It turned out in the successive refinements that the lowest R values, including all measured reflections, are achieved with model III, involving roughly twice as many parameters as used in model I. A significance test on the crystallographic R factors (Hamilton, 1965) indicates that the slight improvement of the R factors of the rigid-body and Frenkel models is not significant compared to the phenomenological split-atom model.*

* Lists of parameters and agreement factors of least-squares models and structure factors have been deposited with the IUCr (Reference: SH0067). Copies may be obtained through The Managing Editor, International Union of Crystallography, 5 Abbey Square, Chester CH1 2HU, England.

Table 2. *Results of the structure refinement of $[Co(NH_3)_6](PF_6)_2$ at room temperature with model III*

Fractional atomic coordinates and equivalent isotropic displacement parameters (Å^2)

	Occupancy	x	y	z	U_{eq}
Co	1.00	0.0000	0.0000	0.0000	0.030 (3)
P	1.00	0.2500	0.2500	0.2500	0.0293 (9)
F	0.25	0.2489 (18)	0.2640 (21)	0.3794 (4)	0.094 (5)
N	1.00	0.1838 (2)	0.0000	0.0000	0.0424 (8)
H1	0.250	0.2139 (26)	−0.0833 (14)	0.0000	0.057 (10)
H2	0.125	0.2276 (27)	0.0437 (15)	0.0633 (22)	0.038 (7)
H3	0.125	0.2066 (26)	0.0361 (13)	−0.0775 (14)	0.041 (6)

Anisotropic displacement parameters (Å^2)

	U_{11}	U_{22}	U_{33}	U_{23}	U_{13}	U_{12}
Co	0.030 (3)	0.030 (3)	0.030 (3)	0.000	0.000	0.000
P	0.0293 (9)	0.0293 (9)	0.0293 (9)	0.000	0.000	0.000
F	0.071 (4)	0.165 (14)	0.045 (2)	−0.049 (7)	0.000 (6)	0.004 (6)
N	0.0321 (10)	0.0476 (11)	0.0476 (11)	0.000	0.000	0.000
H1	0.086 (20)	0.045 (7)	0.039 (14)	0.000	0.000	0.017 (10)
H2	0.032 (13)	0.045 (12)	0.037 (13)	0.019 (11)	−0.006 (10)	−0.003 (12)
H3	0.029 (12)	0.043 (14)	0.052 (10)	−0.011 (10)	−0.002 (8)	−0.026 (6)

Refinement on F^2; $R[F^2 > 2\sigma(F^2)] = 0.0526$; $wR(F^2) = 0.1247$; $S = 1.153$; restrained $S = 1.119$; 182 reflections, 42 parameters, 9 restraints; weighting scheme: $w = 1/[\sigma^2 F_o^2 + (0.0796P)^2]$, where $P = (F_o^2 + 2F_c^2)/3$. Extinction correction: $F_c^* = kF_c[1 + 0.001\chi F_c^2\lambda^3/\sin(2\theta)]^{-1/4}$; extinction coeffficient $\chi = 0.0028$ (17).

Table 3. *Results of the structure refinement of $[Co(NH_3)_6](PF_6)_2$ at 30 K with model 0Y*

Fractional atomic coordinates and equivalent isotropic displacement parameters (Å^2)

	Occupancy	x	y	z	U_{eq}
Co	1.00	0.0000	0.0000	0.0000	0.0055 (3)
P	1.00	0.2500	0.2500	0.2500	0.0041 (9)
F	1.00	0.38655 (8)	0.2500	0.2500	0.0112 (3)
N	1.00	0.18708 (7)	0.0000	0.0000	0.0091 (8)
H1	0.25	0.2200 (9)	0.0000	0.0804 (13)	0.018 (4)
H2	0.25	0.2199 (5)	0.0705 (7)	−0.0397 (7)	0.024 (4)

Anisotropic displacement parameters (Å^2)

	U_{11}	U_{22}	U_{33}	U_{23}	U_{13}	U_{12}
Co	0.0055 (11)	0.0055 (11)	0.0055 (11)	0.000	0.000	0.000
P	0.0041 (4)	0.0041 (4)	0.0041 (4)	0.000	0.000	0.000
F	0.0055 (4)	0.0140 (4)	0.0140 (4)	0.0004 (3)	0.000	0.000
N	0.0075 (5)	0.0099 (3)	0.0099 (3)	0.000	0.000	0.000
H1	0.025 (3)	0.012 (10)	0.017 (3)	0.000	−0.008 (2)	0.000
H2	0.027 (2)	0.026 (5)	0.018 (8)	0.006 (6)	0.003 (2)	−0.007 (2)

Refinement on F^2; $R[F^2 > 2\sigma(F^2)] = 0.0233$; $wR(F^2) = 0.0587$; $S = 1.111$; restrained $S = 1.096$; 174 reflections, 28 parameters, 6 restraints; weighting scheme: $w = 1/[\sigma^2 F_o^2 + (0.0357P)^2 + 6.2379P]$, where $P = (F_o^2 + 2F_c^2)/3$. Extinction correction: $F_c^* = kF_c[1 + 0.001\chi F_c^2\lambda^3/\sin(2\theta)]^{-1/4}$; extinction coeffficient $\chi = 0.0035$ (5).

Considering the structural parameters for the Co, N, P and F atoms, there is no significant difference between all refined models at both temperatures. All temperature parameters have considerably diminished at 30 K.

The different models for the hydrogen density reveal that it is concentrated on a plane that is perpendicular to the respective Co—N axis.

From the refined parameters of the split-atom models, we determined the distance h_{NH_3} between the N ion and the intersection of the fourfold axis with the proton plane. If no tumbling is present, h should reflect the height of the ammonia pyramid. We find at 295 K $h_{NH_3}^{295\,K} = 0.387$ (5) and at 30 K $h_{NH_3}^{30\,K} = 0.386$ (3) Å. In addition, the distance of the protons from the fourfold axis r_p should correspond to the rotational radius of the ammonia molecule. We find $r_p^{295\,K} = 0.893$ (12) and $r_p^{30\,K} = 0.919$ (3) Å. Both h_{NH_3} and r_p turned out to be independent of the underlying split-atom model. They are in good agreement with the NH_3 geometry in the gas phase [$h_{NH_3} = 0.37$, $r_p = 0.94$ Å (Weast, 1985)]

and correspond well with those given by Eckert & Press (1980) for the ammonia molecule in solid $[Ni(NH_3)_6]I_2$ [$h_{NH_3} = 0.38\,(5)$, $r_p = 0.895\,(20)$ Å]. Selected geometric distances for the different models are given in Table 4.

The importance of the parametric models discussed above follows from the stability of the phases of the calculated structure factors, *i.e.* their independence with respect to the parameters refined from different models. 178 out of 182 and 170 out of 172 measured reflections from the two data sets, respectively, could be phased unambiguously. The remaining reflections were ignored in the successive density reconstruction.

Table 4. *Selected geometric parameters (Å)*

Temperature	RT	RT	30 K	30 K
Model	III	I	0*Y*	I
Co—N	2.195 (2)	2.197 (2)	2.199 (1)	2.199 (1)
P—F	1.555 (4)	1.559 (4)	1.605 (1)	1.605 (1)
N—H_i	1.057 (9)	0.974 (12)	1.021 (14)	0.996 (3)
H_i—H_j	1.702 (16)	–	1.637 (34)	–
h_{NH3}	0.385 (31)	0.387 (5)	0.387 (7)	0.386 (3)
r_p	0.978 (19)	0.893 (12)	0.944 (11)	0.919 (3)

4. Proton-density distribution

From the measured structure factors, together with the stable 'model-independent' phases, one may expect to obtain a 'model-free' observed scattering density, provided that the linear inverse Fourier transform can be handled satisfactorily. For comparison, we calculated the scattering density by standard Fourier transformation and by MaxEnt reconstruction. The latter involved a discretization of the unit cell into a 128 × 128 × 128 grid. Figs. 3 and 4 show cuts through the $[Co(NH_3)_6]$ octahedron parallel to the face of the unit cube at $z = 0$ and $z = z_H$, where the maximum proton density occurs. The reduction of series-termination effects in the MaxEnt reconstruction is clearly visible for both data sets.

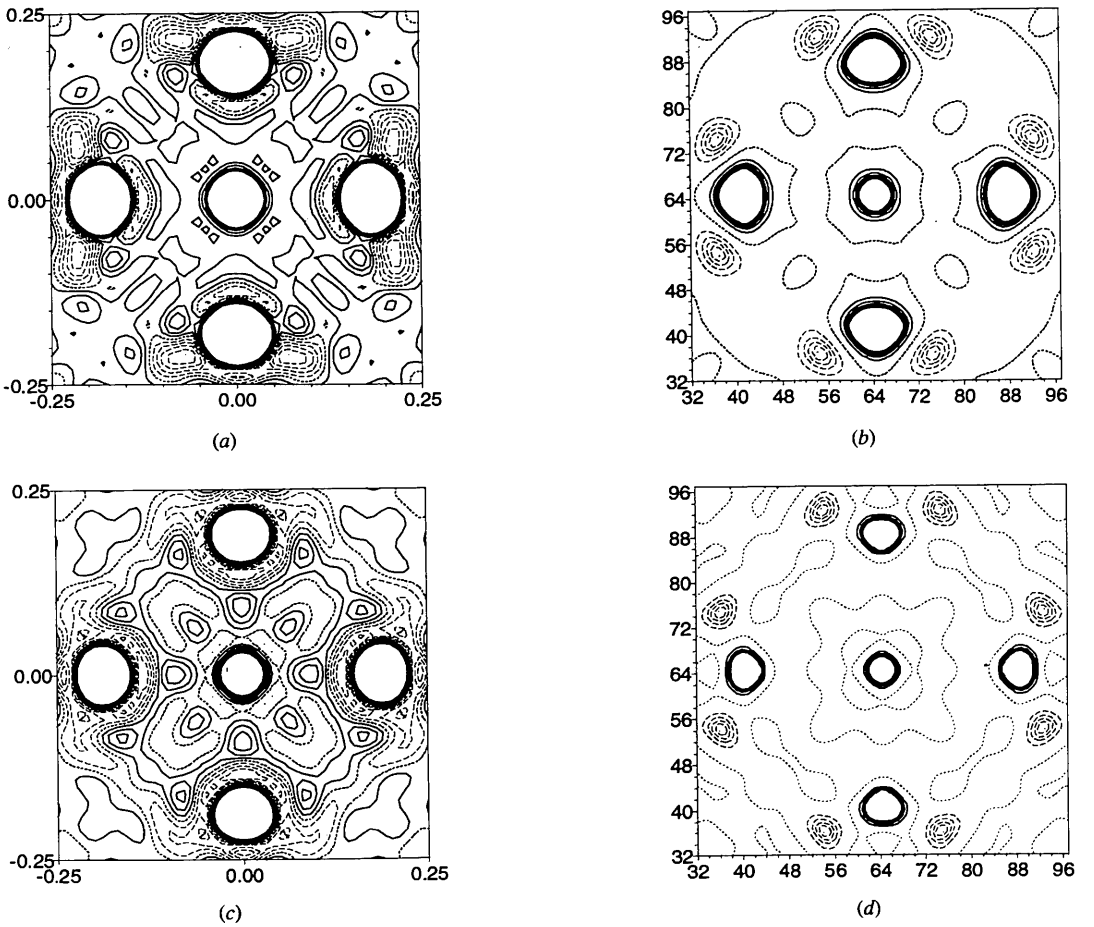

Fig. 3. Cuts through the $[Co(NH_3)_6]$ cluster at $z = 0$. Negative densities are shown as dashed lines, zero level is dotted. (*a*) Fourier density, 295 K; (*b*) MaxEnt density, 295 K; (*c*) Fourier density, 30 K; (*d*) MaxEnt density, 30 K. x and y values in the MaxEnt maps are given in units of $\Delta = 1/128a$. Ten level lines are drawn at intervals of 20% of the minimum density value.

In the Fourier reconstruction, series-termination effects result in a modulation of the whole density with an amplitude that is comparable with the maximum of the proton density. This leads to spurious negative density values. In contrast, in the MaxEnt reconstruction, no negative density values show up except where the proton density is supposed to be.

In addition, all features of the density are broadened in the Fourier map. As a consequence of this broadening combined with thermal motion, some nitrogen density shows up in the centre of Fig. 4 and is thus superimposed on the proton density. Actually, the equilibrium position of the centre of mass of the N atom lies about $h_{NH_3} = 0.4$ Å below the proton plane. At 30 K, owing to the low thermal motion and the high resolution of the MaxEnt reconstruction, nitrogen and proton density is well separated (Fig. 3*d*).

Thus, despite the fact that the use of MaxEnt remains subject to caution (Jauch & Palmer, 1993; Jauch, 1994), it seems to be more appropriate than the standard Fourier transform for our purpose here, namely to model better the hydrogen density and the potential.

From Fig. 3, it is obvious that the proton density is concentrated in planes perpendicular to the fourfold axis. This indicates that large tumbling motions of the NH_3 top do not occur. In addition, Fig. 4 shows that the observed proton density is nearly circular, with a weak tetragonal distortion at both temperatures.

5. Orientational potential

Since the proton density is observed to be concentrated in a plane perpendicular to the Co—N axis, we reduce the dynamical problem of the NH_3 motion to the motion of an H_3 triangle in a plane. In order to explain the observed proton density, we assume a time-independent two-dimensional anharmonic mean crystal potential V_{Cr}. Our basic assumption is that V_{Cr} is an effective potential that contains all time-independent contributions due to neighbours acting upon the reference NH_3 group.

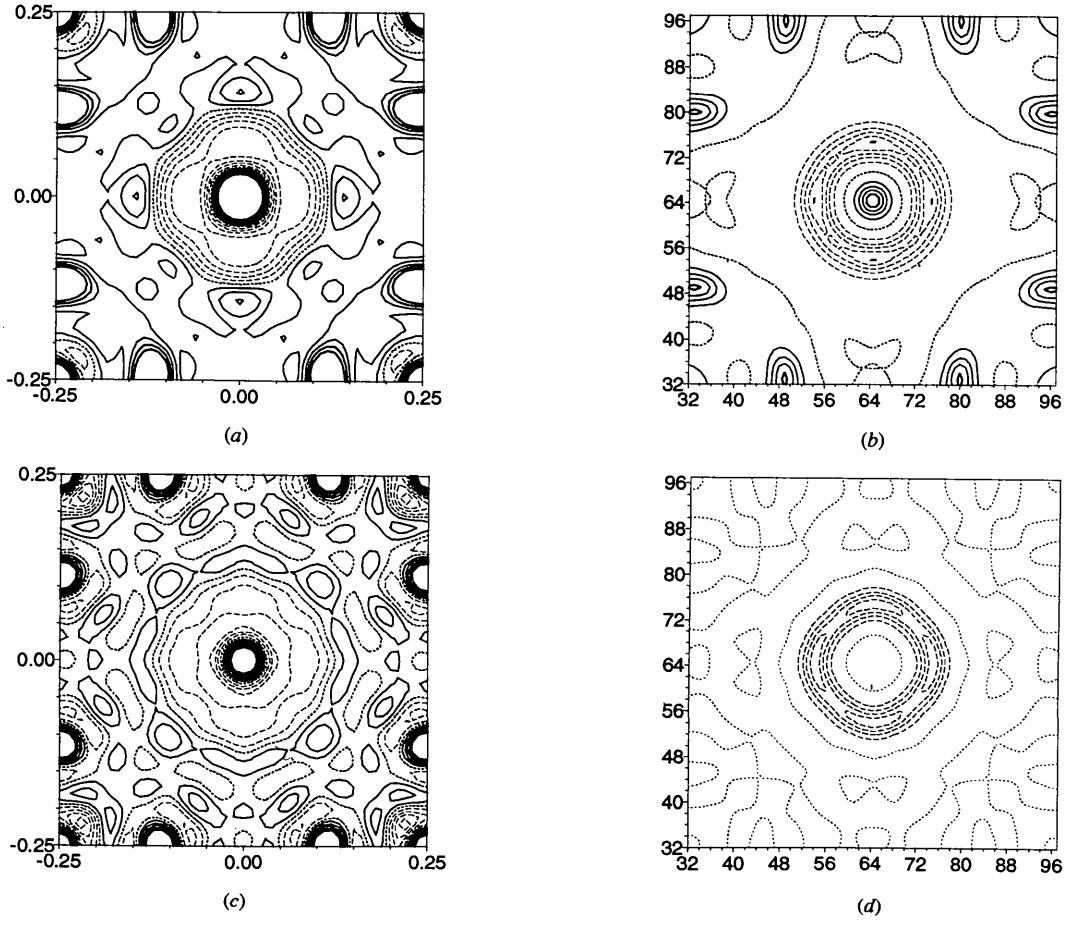

Fig. 4. Cuts through the hydrogen density at $z = z_H$. Hydrogen scattering densities (negative) are shown as dashed lines, zero level is dotted. Clearly visible is the pseudo-eightfold symmetry established by the eight nearest-neighbour F atoms. (*a*) Fourier density, 295 K; (*b*) MaxEnt density, 295 K; (*c*) Fourier density, 30 K; (*d*) MaxEnt density, 30 K. x and y values in the MaxEnt maps are given in units of $\Delta = 1/128a$. Ten level lines are drawn at intervals of 20% of the minimum density value.

It therefore must possess the symmetry of the two-dimensional point group $4mm$ according to the site symmetry $4mm$ on the fourfold axis.

$$V_{Cr}(r,\varphi) = \tfrac{1}{2}Ar^2 + \tfrac{1}{4}Br^4\cos 4\varphi + \tfrac{1}{4}Cr^4. \quad (1)$$

(r,φ) is the actual position of one H atom (Fig. 5). This anharmonic potential couples the rotational motion of the H_3 triangle to its centre-of-mass motion. The parameter B denotes the strength of the coupling whereas B and C measure the anharmonicity of the potential.

The H_3 triangle is assumed as rigid, and so (r,φ) depends on the centre-of-mass distance R_c and the polar angle φ_c of the H_3 group, and on the proton setting angle β (Fig. 5). The effective molecular potential for one setting of the H_3 triangle is given by the sum of the single-particle potentials of each proton:

$$V_M(R_c,\varphi_c,\beta) = \sum_{p=0}^{2} V_{Cr}(r_p,\varphi_p). \quad (2)$$

The Boltzmann probability for one configuration (R_c,φ_c,β) is known to be

$$\rho(R_c,\varphi_c,\beta) = Z^{-1}\exp[-V_M(R_c,\varphi_c,\beta)/kT], \quad (3)$$

where Z is the partition function. The scattering density $\rho(x,y)$ observed is a configurational average:

$$\rho(x,y) = 3Z^{-1}\exp[-V^0_{Cr}(x,y)/kT] \times \int \exp[-(V^1_{Cr}+V^2_{Cr})/kT]\,d\gamma. \quad (4)$$

Thus, the mean crystal potential may be determined by a least-squares analysis of the observed densities. Refined parameters were the three potential parameters A, B, C, a scale factor and the distance d_p of the three protons from their center of mass. In addition, a constant density contribution c_0 is added in the refinement. As input data, we used the central part of the two-dimensional maps given in Figs. 4(*b*), (*d*) and we assigned equal weights to all observed density values. The results of the potential refinement are given in Table 5. It should be mentioned that the standard deviations of the parameters given are only low estimates, since they do not incorporate the standard deviation in the MaxEnt density. Figs. 6 and 7 illustrate the observed and calculated proton scattering densities at both temperatures.

Table 5. *Results of the potential refinement*

	295 K	30 K
A (K Å^{-2})	−548.3 (5)	−142.16 (2)
B (K Å^{-4})	−62.9 (27)	−19.12 (17)
C (K Å^{-4})	1972.6 (163)	332.24 (56)
d_p (Å)	0.9689 (5)	0.9437 (2)
Scale	−89.9 (2)	−37.72 (4)
Density background	−0.218 (8)	−0.037 (6)
R^p	0.091	0.044

$$R^p = \frac{\sum_i^{Nx}\sum_j^{Ny}|\rho_o(x_i,y_j) - \rho_c(x_i,y_j)|}{\sum_i^{Nx}\sum_j^{Ny}|\rho_o(x_i,y_j)|}.$$

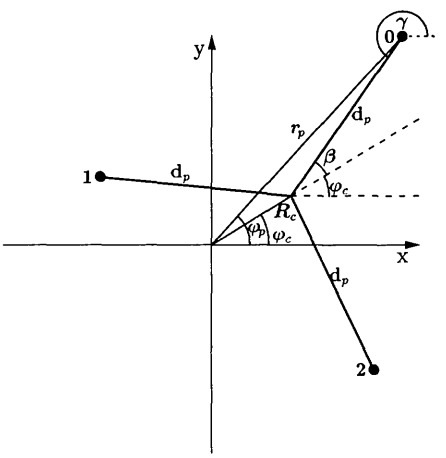

Fig. 5. Geometric quantities defining the model.

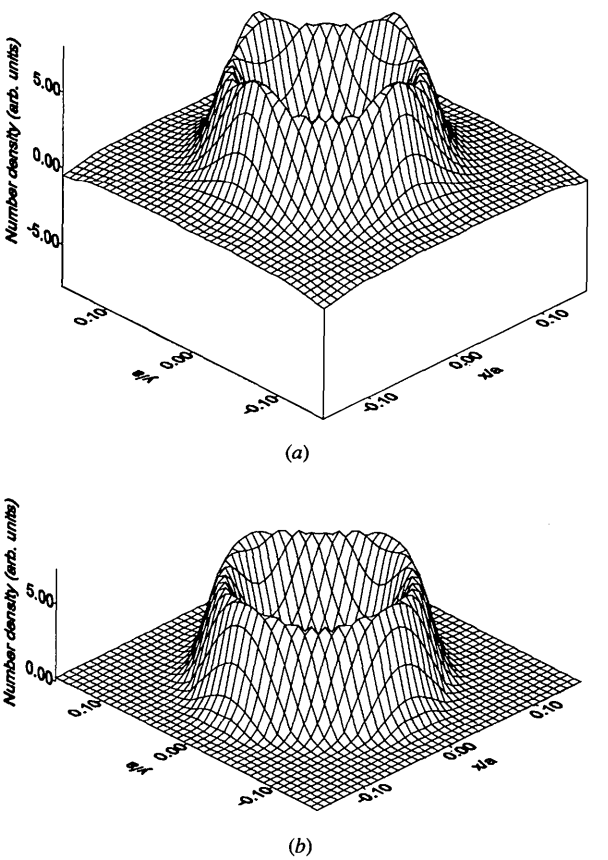

Fig. 6. (*a*) Observed and (*b*) calculated proton densities at 295 K. x and y values are given in units of $\Delta = 1/128a$.

The reported R values R^p of Table 5 may not be compared to the R values of the structure refinement (Tables 2 and 3), which describe the agreement between the models for the total structure and the data, whereas the R^p refer only to the pure proton density. For comparison, we calculated the corresponding R value for the two-dimensional nuclear density derived from the *SHELX* refinement at 30 K and found $R = 0.12$. The reason for the discrepancy in the R values is obvious: Any deficiencies of the models describing the proton density will contribute only in a minor fashion to the total R values of the structure refinement. Nevertheless, from the calculation of the scattering-length density of the total structure (H atoms plus P, F, N atoms) in the whole unit cell, it is possible in principle to derive calculated structure factors by a Fourier transform, which in turn may be compared to the observed ones.

The resulting mean crystal potential at 295 K, shown in Fig. 8, is nearly circular with a very weak tetragonal distortion. The main contribution is due to the rotational symmetric anharmonic term in (1), $\sim Cr^4$, whereas the coupling parameter B is found to be relatively small: B stands for a tetragonal modulation of $V_{Cr(r,\varphi)}$. From Figs. 4(*b*), (*d*), it is, however, clear that the F atoms surrounding an NH_3 group form a nearly regular octagon.

Details of the underlying dynamics that lead to the observed proton density distribution are now easily obtained from the effective molecular potential (2), which may be evaluated as a function of (R_c, φ_c, β):

$$V_M(R_c, \varphi_c, \beta) = V^0 + V^R(R_c) + V^W(R_c, \varphi_c, \beta) \quad (5)$$

with

$$V^0 = 3[\tfrac{1}{2}Ad^2 + \tfrac{1}{4}Cd^4] \quad (6)$$

$$V^R(R_c) = 3[(\tfrac{1}{2}Ad + \tfrac{1}{4}Cd^2)R_c^2 + \tfrac{1}{4}CR_c^4] \quad (7)$$

$$V^W(R_c, \varphi_c, \beta) = 3[Bd^3 \cos(4\varphi_c + 3\beta) + \tfrac{1}{4}BR_c^4 \cos(4\varphi_c)]. \quad (8)$$

V^0 is simply a zero-point shift of the potential. V^R includes all the rotationally symmetric parts, whereas $V^W(R_c, \varphi_c, \beta)$ represents the rotation–translation coupling. Consequently, it is dominated by the parameter B and shows explicitly periods of 90° in terms of φ_c and 120° in terms of β. With given $R_c = 0$, V_M is independent of both φ_c and β. With increasing R_c, the three- and fourfold periodicities show up and the absolute potential minima occur under a defined value $R_{c,\min} = R_m \neq 0$. With the potential parameters given in Table 5, the absolute potential minimum in V_M occurs at $\varphi_c = \beta = 0$ and $R_m^{295\,K} = 0.018$ Å ($R_m^{30\,K} = 0.036$ Å). $V_M(R_m, \varphi_c, \beta)$ is given in Fig. 9. The absolute potential minimum along the valleys is only very weakly pronounced compared to the valleys showing up in Fig. 9. At both temperatures, the hindrance potential for 120° jumps and the potential barriers that the molecules have to overcome if they move from one potential minimum to another are very weak compared with the thermal energy kT of the measurement.

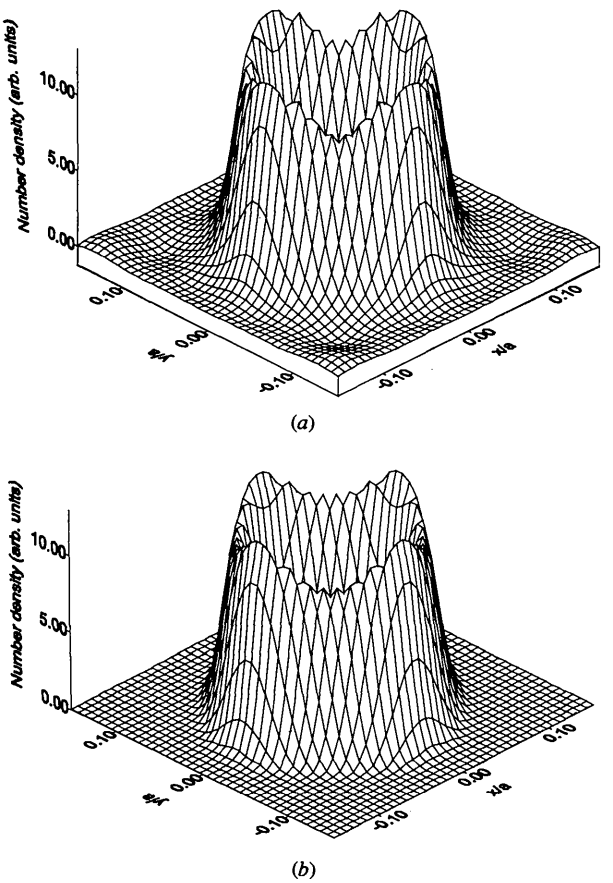

Fig. 7. (*a*) Observed and (*b*) calculated proton densities at 30 K. x and y values are given in units of $\Delta = 1/128a$.

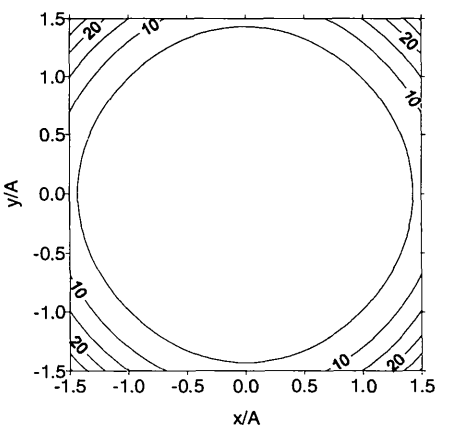

Fig. 8. Mean crystal potential V_{Cr} calculated with the potential parameters at 295 K given in Table 3. Potential levels are in units of $kT = 295$ K.

As is evident from (6), a simple rotation of the molecule around the fourfold axis would imply $R_c = R_m = 0$ and $V_M = V^0$. Our calculated values clearly demonstrate that the main contribution to the molecular potential essentially results from the harmonic part of (7) and therefore the dynamics of the H_3 triangle is very close to free rotation.

6. Conclusions

Maximum-entropy reconstruction combined with a preliminary phasing of the absolute values of the observed structure factors yields a powerful tool for direct observation of the density of rotating molecules. By comparison with standard Fourier synthesis, the great success of MaxEnt is due to its huge reduction of termination effects as well as its noise-suppressing role.

In $[Co(NH_3)_6](PF_6)_2$, the observed proton density at 295 and 30 K is concentrated in planes perpendicular to the respective Co—N axis. The distance from the proton plane to the N site reflects the height of an undistorted ammonia pyramid. Thus, large tumbling motion of the ammonia molecules is ruled out. In the proton plane, the proton density shows up to be nearly circular with a weak tetragonal distortion. This observation is explained by an anharmonic potential that is adapted to the site symmetry *4mm*.

The hindrance potential is found to be very weak and the dynamics of the protons in $[Co(NH_3)_6](PF_6)_2$ is close to uniaxial free rotation.

We make a final remark about the large differences between the two sets of potential parameters (Table 5) found at 295 and 30 K: they are due to our *Ansatz* (3), (4) for the densities. Equations (3) and (4) are of course Boltzmann densities that are valid only at and above room temperature. At 30 K, this approximation breaks down and quantum statistics must be used. One may demonstrate this breakdown, for example, from the rotational energy of a one-dimensional rotator $E_l = l^2B$, with $l = 0, \pm1, \pm2, \ldots$, and the rotational constant $B = \hbar^2/I$, where I is the moment of inertia for rotations of the NH_3 group about its trigonal axis. We find $B = 8.6$ K for NH_3, and so from $E_l \simeq kT$ we find all levels having $l \lesssim 2$ well occupied at 30 K and $l \lesssim 7$ at 295 K. The low number of levels occupied at 30 K forces definitively a quantum-statistical treatment of the problem: we are working out the programs at present, which turns out to be lengthy. So, for the time being, we interpret *A*, *B*, *C* at 295 K as representing a true potential, whereas *A*, *B*, *C* at 30 K represent an operational potential that is defined by the 'illegal' application of the Boltzmann approximation at low temperatures.

Nevertheless, the central issue of this paper, namely the first direct geometrical evidence for nearly free rotation of the NH_3 group at 30 K as well as at 295 K, is not affected by this cautious remark.

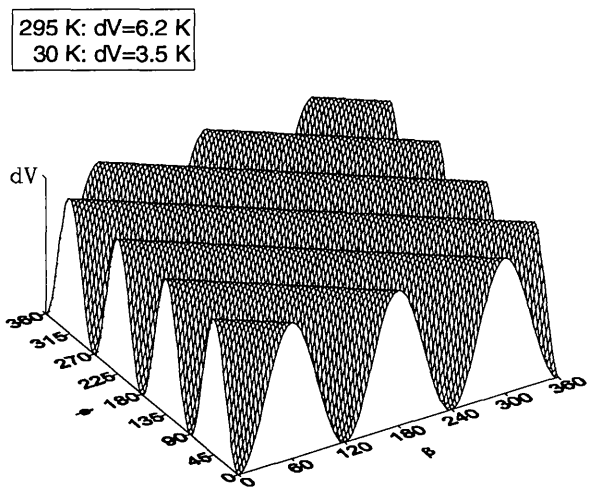

Fig. 9. Effective molecular potential $V_M(R_m, \varphi, \beta)$ for fixed centre-of-mass radius. A jump across a maximum corresponds to a rotation of the molecule by 120° about an axis passing through its centre of mass. The low heights of the potential ridges cannot hinder free rotation.

This investigation was supported by DFG (project PR44/7-1), and by the BMFT (projects 03-HA3AAC and 03-PR3TUE-0).

References

Bates, A. R. & Stevens, K. W. H. (1969). *J. Phys. C*, **2**, 1573–1585.
Eckert, J. & Press, W. (1980). *J. Chem. Phys.* **73**, 451–460.
Hamilton, W. C. (1965). *Acta Cryst.* **18**, 502–510.
Janik, J. A., Janik, J. M., Migdal-Mikuli, A., Mikuli, E. & Otnes, K. (1991). *Physica (Utrecht)*, **B168**, 45–52.
Jauch, W. (1994). *Acta Cryst.* **A50**, 650–652.
Jauch, W. & Palmer, A. (1993). *Acta Cryst.* **A49**, 590–591.
Kearley, G. J., Blank, H. & Cockcroft, J. K. (1987). *J. Chem. Phys.* **86**, 5989–5993.
Papoular, R. & Gillon, P. (1990*a*). *Neutron Scattering Data Analysis 1990*, edited by N. Johnson. *Inst. Phys. Conf. Ser.* **107**, 101–116.
Papoular, R. & Gillon, P. (1990*b*). *Europhys. Lett.* **13**, 429–434.
Papoular, R. J., Prandl, W. & Schiebel, P. (1992). *Maximum Entropy and Bayesian Methods, Seattle, 1991*, edited by C. R. Smith, G. J. Erickson & P. Neudorfer, pp. 359–376. Dordrecht: Kluwer.
Sakata, M., Uno, T., Takata, M. & Howard, C. J. (1993). *J. Appl. Cryst.* **26**, 159–165.
Schiebel, P., Hoser, A., Prandl, W., Heger, G., Paulus, W. & Schweiss, P. (1995). *J. Phys. Condens. Matter*, **6**, 10989–11005.
Sheldrick, G. M. (1993). *SHELXL93. Program for Crystal Structure Determination*. University of Cambridge, England.
Weast, R. C. (1985). *Handbook of Chemistry and Physics*, 66th ed. Oxford: CRC Press.